

PERMUTATION-BASED TRUE DISCOVERY PROPORTIONS FOR FMRI CLUSTER ANALYSIS

BY ANGELA ANDREELLA¹, JESSE HEMERIK^{2,*}, WOUTER WEEDA^{3,†}, LIVIO FINOS^{4,‡} AND JELLE GOEMAN^{5,§}

¹*Department of Statistical Sciences, University of Padova* angela.andreella@stat.unipd.it

²*Biometris, Wageningen University and Research* jesse.hemerik@wur.nl

³*Methodology and Statistics Unit, Department of Psychology, Leiden University* w.d.weeda@fsw.leidenuniv.nl

⁴*Department of Developmental Psychology and Socialization, University of Padua* livio.finos@unipd.it

⁵*Biomedical Data Sciences, Leiden University Medical Center* j.j.goeman@lumc.nl

We develop a general permutation-based closed testing method to compute a simultaneous lower confidence bound for the true discovery proportions of all possible subsets of a hypothesis testing problem. It is particularly useful in functional Magnetic Resonance Imaging cluster analysis, where it is of interest to select a cluster of voxels and to provide a confidence statement on the percentage of truly activated voxels within that cluster, avoiding the well-known spatial specificity paradox. We offer a user-friendly tool to find the percentage of true discoveries for each cluster while controlling the familywise error rate for multiple testing and taking into account that the cluster was chosen in a data-driven way. Permutation theory adapts to the spatial correlation structure that characterizes functional Magnetic Resonance Imaging data and therefore gains power over parametric approaches.

1. Introduction. Functional Magnetic Resonance Imaging (fMRI) is the most frequently used technique to understand which regions of the human brain are activated as a consequence of a stimulus. Brain activation is measured as the correlation between the sequence of cognitive stimuli and the sequence of measured blood oxygenation levels (BOLD). The brain image is composed of voxels, and for each of these, we can test for significant neural activity with respect to an inactive region null hypothesis. Consequently, inference on the percentage of activated voxels in selected brain regions is of interest. Approximately 300,000 voxels are analyzed, so the resulting multiple testing problem has roughly 300,000 statistical tests.

Controlling Type I error at the voxel level is conservative (Nichols and Hayasaka, 2003), since, e.g., the Bonferroni approach does not consider the correlation data structure. Therefore, cluster-extent based thresholding was developed to analyze the data at the level of clusters of contiguous voxels. This method is less conservative than voxel-wise inference since it exploits the spatial nature of the signal. However, the assumptions behind this method require a very high cluster-forming threshold, resulting in small clusters (Eklund, Nichols and Knutsson, 2016). Moreover, the method suffers from the spatial specificity paradox (Woo, Krishnan and Wager, 2014). Since the method tests the hypothesis that none of the voxels in the cluster are active, rejecting this null hypothesis only allows the claim that there is at least one active voxel inside the cluster. The number of active voxels and their spatial location remains unknown, and doing follow-up inference inside the cluster (“drilling down”) leads to a double-dipping problem and inflated Type I error rate (Kriegeskorte et al., 2009).

Keywords and phrases: True Discovery Proportion, Permutation Test, Multiple Testing, Selective Inference, fMRI Cluster Analysis.

These problems motivated [Rosenblatt et al. \(2018\)](#) to propose All-Resolution Inference (ARI), a method to compute the lower confidence bound for the true discovery proportion (TDP) simultaneously for all possible sets, e.g., all clusters of voxels. Simultaneous control permits users to drill down within clusters while maintaining error guarantees, thus resolving the spatial specificity paradox. ARI is based on the approach proposed by [Goeman and Solari \(2011\)](#) using closed testing ([Marcus, Peritz and Gabriel, 1976](#)) with local Simes test ([Simes, 1986](#)) to control the familywise error rate (FWER). The closed testing method has an exponential computational load in general; nevertheless, for this specific case [Goeman et al. \(2019\)](#), and [Meijer et al. \(2019\)](#) proposed a fast and exact linear time short-cut. ARI relies on the Simes inequality, assuming positive regression dependency on subsets (PRDS) ([Sarkar, 2008](#)). While the Simes inequality can be assumed to be valid for fMRI data ([Nichols and Hayasaka, 2003](#)), it can be conservative under strong positive dependence. This makes the method inefficient in the neuroimaging data framework since brain measurements have strong spatial dependence due to both physics and physiology.

Permutation tests assume only exchangeability under the null hypothesis ([Pesarin and Salmaso, 2010](#)) and can handle data having any correlation structure, adapting to that correlation structure both to keep type I error control and to gain power. [Hemerik, Solari and Goeman \(2019\)](#) proposed a permutation-based method, related to ARI, that adapts the procedure to the correlation structure of the p -values. However, this method finds TDP only for sets consisting of the smallest k p -values, simultaneously over k , and can therefore not handle spatially defined clusters. Also, the method allows much freedom in the choice of the shape of its rejection curve, and the optimal choice for fMRI data is not clear.

In this paper, we merge the strengths of ARI with the permutation-based method of [Hemerik, Solari and Goeman \(2019\)](#), adapting ARI to use permutations and generalizing the method of [Hemerik, Solari and Goeman \(2019\)](#) to make inference on arbitrary subsets of the hypotheses. The new method provides a lower bound for the TDP for all brain regions, allowing regions of interest to be chosen post-hoc, as in ARI, without compromising familywise error control. By using permutation-based test statistics, the method gains in power compared to the parametric version of ARI because it adapts to the correlation structure. Moreover, permutation tests are robust, as widely demonstrated in the neuroimaging literature ([Eklund, Nichols and Knutsson, 2016](#); [Winkler et al., 2016a,b](#)) and can be used when the parametric assumptions of ARI are not satisfied.

This paper is organized as follows. Section 2 introduces the concept of closed testing based on a critical vector, revisiting results from [Goeman, Hemerik and Solari \(2019\)](#) and [Rosenblatt et al. \(2018\)](#). Then, in Section 3, we combine these results to obtain permutation-based ARI, discussing families of critical curves to be used in Section 4 and which test and permutations we recommend to use in fMRI data in Section 5. Section 6 evaluates the performance of our method in comparison with the parametric version in fMRI data. We validate the method using the resting-state fMRI null data of [Eklund, Nichols and Knutsson \(2016\)](#) in Section 7. Finally, we perform some simulations in Section 8 in order to investigate the shape of the rejection curve in the case of p -values with conservative and anti-conservative structure.

2. Closed testing for false discovery proportions. In this Section, we revisit some results from [Rosenblatt et al. \(2018\)](#) and [Goeman, Hemerik and Solari \(2019\)](#) to introduce notation and to clarify the need for selective inference in fMRI data.

Suppose the brain B , with $|B| = m$, is composed of m voxels, and let 2^B be the collection of all subsets of the brain. Some of the voxels are truly active: let $A \subseteq B$ be the unknown set of all truly active voxels. For a cluster of interest $S \subseteq B$ we want to make inference on $a(S) = |A \cap S|$, i.e., the number of truly active voxels in S , or equivalently the TDP, i.e., $a(S)/|S|$.

We assume that we have computed a test statistic for each voxel i , where $i = 1, \dots, m$, corresponding to the null hypothesis that the voxel is not active. Based on some knowledge or guess of the marginal null distribution of these test statistics we may compute corresponding (parametric) p -values $p_i : \Omega \rightarrow [0, 1]$ where Ω is the sample space of the data X . In the parametric version, we will assume that these p -values will be valid, i.e., stochastically smaller than the uniform distribution of all inactive voxels. For the permutation-based method we emphasize here that, to guarantee FWER control, we do not make any assumptions on the distribution of these p -values. The reason is that it will suffice that the p -values are computed in the same way for all permuted versions of the data (Hemerik, Solari and Goeman, 2019).

We will now revisit simultaneous inference on TDP using closed testing and critical vectors. First, we define a critical vector.

DEFINITION 2.1. A vector l_1, \dots, l_m is a critical vector if and only if

$$(1) \quad \Pr(\cap_{i=1}^{|N|} \{q_{(i)} \geq l_i\}) \geq 1 - \alpha,$$

where $N = B \setminus A$ is the set of inactive voxels, and $q_{(i)}$, $1 \leq i \leq |N|$, are their sorted p -values.

The general parametric version of ARI assumes that, for a chosen error rate $\alpha \in [0, 1]$, there is a critical vector l_1, \dots, l_m , possibly random, expressed as Definition 2.1. If such a critical vector exists, then as a corollary to Lemma 8 from Goeman, Hemerik and Solari (2019) we have the following proposition, which we prove in the supplementary material.

PROPOSITION 1. Let l_i satisfy (1). Then for every $\emptyset \neq S \subseteq B$,

$$(2) \quad \bar{a}(S) = \max_{1 \leq u \leq |S|} 1 - u + |\{i \in S : p_i \leq l_u\}|$$

is a lower $(1 - \alpha)$ confidence bound of $a(S)$, simultaneously for all $S \subseteq B$, that is

$$(3) \quad \Pr(\forall S \subseteq B : \bar{a}(S) \leq a(S)) \geq 1 - \alpha.$$

In ARI, the Simes-based critical vector is $l_i = i\alpha/h$, where h is a random variable that can be calculated using the short-cut defined by Goeman et al. (2019). It is the largest set size of a subset of the brain not rejected by the Simes test.

Figure 1 illustrates computation of $\bar{a}(S)$ as defined in Equation (2), where $|S| = 1000$. In the left part, the length of the dashed black segments are the $z = 1 - u + |\{i \in S : p_i \leq l_u\}|$ with $u \in \{1, \dots, |S|\}$ described in Equation (2), while the solid red segment is the maximum value over u , i.e., the highest distance between the curve of observed p -values and critical vector l_i , e.g., Simes-based. In the right part, we can see the trend of $\bar{a}(S)$ over u . The maximum value of $1 - u + z = 232$ is reached when u equals 97. This implies that $\bar{a}(S) = \max_{1 \leq u \leq |S|} 1 - u + |\{i \in S : p_i \leq l_u\}| = 232$ is a lower confidence bound for the number of true discoveries in S .

The crucial assumption of Proposition 1 is that l_i satisfies (1). In the case of the Simes test used by ARI, this follows from the PRDS assumption, commonly also adopted for the False Discovery Rate (FDR) controlling approach proposed by Benjamini and Hochberg (1995). Although this assumption is commonly accepted in neuroimaging (Nichols and Hayasaka, 2003), the critical values l_1, \dots, l_m can be overly strict if p -values are positively correlated, leading to conservative results. Moreover, the Simes critical vector may also be too strict or too loose if the p -values are not well calibrated.

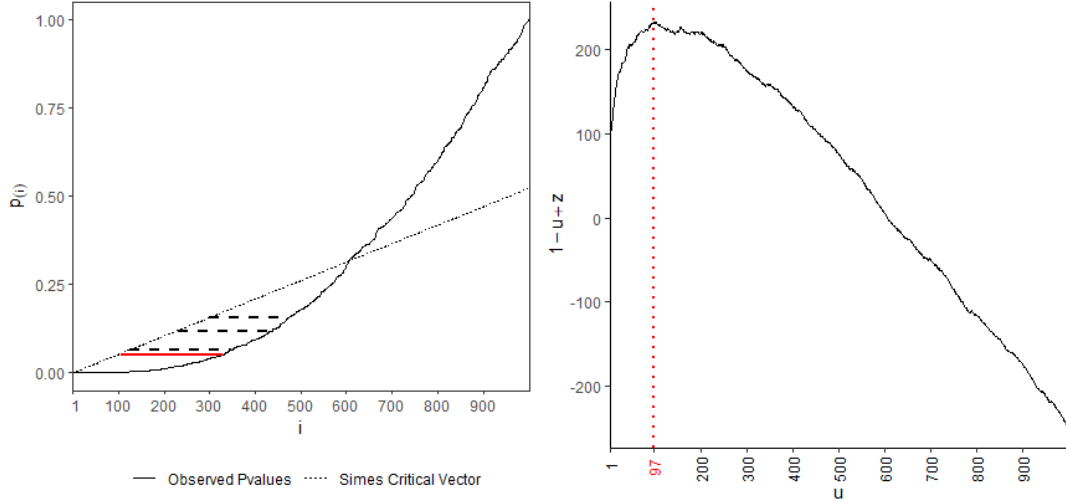


FIG 1. *Left Figure: Example of $\bar{a}(S)$ computation, i.e., the highest horizontal distance between the curve of observed p-values and critical vector, represented by the solid red segment. Right Figure: Example of $\bar{a}(S)$ computation, i.e., the maximum $1 - u + z$ over u .*

3. Permutation-based All-Resolutions Inference. To obtain a critical vector that leads to improved power, we propose a permutation procedure, based on results in [Hemerik, Solari and Goeman \(2019\)](#). The permutation method takes into account the dependence structure of the p-values and, therefore, often leads to a higher critical curve than parametric methods. Moreover, permutation methods not only adapt to the dependence structure but also to the marginal distributions of the p-values. This means that we do not require the null p-values to be uniformly distributed. Instead, we require that the null p-values are exchangeable with the corresponding post-permutation p-values (Assumption 1 in [Hemerik, Solari and Goeman \(2019\)](#)).

Following [Hemerik, Solari and Goeman \(2019\)](#), we consider a group of permutations or sign-flipping transformations or any other data transformation that preserves the distribution of the test statistics under the null hypothesis, such as rotations ([Hemerik, Goeman and Finos, 2020](#)). These are maps from the support of the data distribution to itself. Our method is based on w random permutations or sign-flipping transformations. Let $p_1^1, \dots, p_m^1 = p_1, \dots, p_m$ be the p-values for the real data, and for every $2 \leq j \leq w$, let p_1^j, \dots, p_m^j be the p-values obtained for the j -th random permutation of the data.

Computing all possible permutations could be computationally infeasible, especially in the fMRI framework. However, Proposition 2 of [Hemerik and Goeman \(2018\)](#) states that if the permutation set has a group structure, and $\alpha \in [0/w, 1/w, \dots, (w-1)/w]$, the random permutations reach an exact α level. This means that the α level is exhausted if all hypotheses are true, and the error rate is at most α otherwise.

To obtain the permutation-based critical vector, the user must choose a family of candidate critical vectors. Examples of such candidate vectors are given in Section 4. We suppose that the candidate vectors are indexed by $\lambda_\alpha \in \Lambda \subseteq \mathbb{R}$, so that $l(\lambda_\alpha)$ denotes the candidate vector corresponding to λ_α . The family of candidate vectors is thus $\mathcal{F} = \{l(\lambda_\alpha) : \lambda_\alpha \in \Lambda\}$. We assume that the family of candidate vectors is monotone, in the sense that if $\lambda_\alpha^1, \lambda_\alpha^2 \in \Lambda$ and $\lambda_\alpha^1 \leq \lambda_\alpha^2$, then $l_i(\lambda_\alpha^1) \leq l_i(\lambda_\alpha^2)$ for every $1 \leq i \leq m$.

We define the permutation-based critical vector to be $l(\lambda_\alpha)$, where

$$(4) \quad \lambda_\alpha = \sup\{\lambda_\alpha \in \Lambda : w^{-1}|\{1 \leq j \leq w : p_i^j \geq l_i(\lambda_\alpha) \ \forall i\}| \geq 1 - \alpha\}.$$

By [Hemerik, Solari and Goeman \(2019\)](#), the following holds.

THEOREM 3.1. *The vector $l(\lambda_\alpha)$ is a critical vector, i.e., it satisfies (1) of Definition 2.1.*

The λ_α -calibration permits to incorporate the unknown dependence structure of the data into the choice of the critical vector. As seen from (4), the vector λ_α is computed in such a way that for at least $(1 - \alpha)100\%$ of the permutations, all p-values lie above it. This is illustrated in Figure 2, considering a random sample of 100 permutation curves. The λ_α parameter tends to be lower, if many null hypotheses are false, being "optimal" if Definition (4) considers only $p_i \in B \setminus A$, i.e., the set of true null hypotheses.

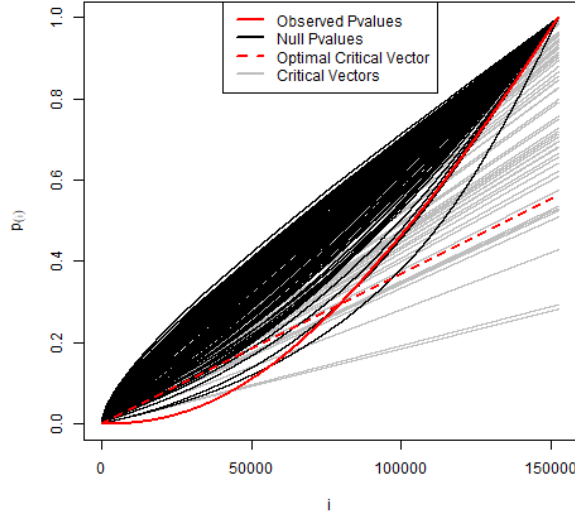


FIG 2. Example of $l_i(\lambda_\alpha)$ computation using $\alpha = 0.10$. The dashed red line represents the highest critical curve than the gray ones, such that the $\alpha\%$ p-values distribution (black curves plus red one) is below it.

The method can be uniformly improved by its step-down version ([Hemerik, Solari and Goeman, 2019](#)), where the confidence envelope is defined as the maximum confidence bound computed in the complementary set of rejection set having cardinality equal to the upper bound of the number of true positives found in the previous iteration. Therefore, the improvement is substantial only when the number of detectable false hypotheses is large.

We use the critical vector $l_i(\lambda_\alpha) \in \mathcal{F}$ in Proposition 1 instead of the Simes-based one employed in ARI to gain power in computing $\bar{a}(S)$. The computation time for $\bar{a}(S)$ is primarily related to the calculation of the permutation p-values distribution and on sorting them. Our algorithm, written in C++, takes around 0.3 seconds when considering 2000 variables and 20 observations for 1000 permutations. The computation time comes from a device with a processor having 1.8 GHz CPU and 16 GB of RAM. We did not consider the step-down improvement since we found it to be computationally infeasible for fMRI data. Performing the step-down approach requires that the l_i vector must be recomputed for exponentially many $S \subseteq B$. Also, as we will see in Section 6, the number of detectable false null hypotheses is not large, so the gain in power of the step-down method was expected to be small.

4. Choice of family of curves. In the previous Section we consider a general family \mathcal{F} of candidate vectors $l(\lambda_\alpha)$, $\lambda_\alpha \in \Lambda$. Here we will discuss several examples of such families, which we considered in the application later in the paper.

The first family \mathcal{F} that we consider is inspired by Simes' probability inequality (Simes, 1986). The vectors are obtained by multiplying and shifting the Simes' critical vector. We denote the shift by $\delta \in \mathbb{R}^+$. For every such δ , we have a different family, indexed by $\lambda_\alpha \in \mathbb{R}^+$. The candidate critical vector $l(\lambda_\alpha)$ is defined by

$$(5) \quad l_i(\lambda_\alpha) = \frac{(i - \delta)\lambda_\alpha}{m - \delta}.$$

The shift parameter δ can be used to determine how sensitive the critical vector $l(\lambda_\alpha)$ will be to the smallest p-values. The parametric Simes-based approach corresponds to $\delta = 0$ and $\lambda_\alpha = \alpha$. We gain over the that approach only if the λ_α value is greater than α .

Regarding the choice of δ , note that $l_i(\lambda_\alpha) \leq 0$ for $i \leq \delta$. As a consequence, we will find $\bar{a}(S) \leq |S| - \delta$, and $\bar{a}(S) = 0$ for all S with $|S| \leq \delta$. The value of δ therefore corresponds to the minimum size of a cluster that we are interested in detecting. To compensate, methods with large δ will often have a steeper slope λ_α and consequently have more power for detecting large clusters.

The second example that we consider is a family \mathcal{F} of candidate vectors that are derived from the asymptotically optimal rejection curves (AORC) considered in Finner, Dickhaus and Roters (2009) to control the FDR in an asymptotic Dirac uniform setting. Again we add a shift parameter $\delta \in \mathbb{R}^+$ as above, and we have a different family of candidate vectors for each δ . The calibration parameters lie in $\Lambda \subseteq \mathbb{R}$. The candidate critical vector $l(\lambda_\alpha)$ is defined by

$$(6) \quad l_i(\lambda_\alpha) = \frac{(i - \delta)\lambda_\alpha}{(m - \delta) - (i - \delta)(1 - \lambda_\alpha)}.$$

Our third example is related to the Higher Criticism method proposed by Donoho and Jin (2004). The candidate vectors are indexed by $\lambda_\alpha \in \Lambda \subseteq \mathbb{R}$ and are given by

$$(7) \quad l_i(\lambda_\alpha) = \frac{2i + \lambda_\alpha^2 - \sqrt{(2i + \lambda_\alpha^2)^2 - 4i^2(m + \lambda_\alpha^2)/m}}{2(m + \lambda_\alpha^2)}.$$

Finally we, we consider the family of candidate vectors $l(\lambda_\alpha)$ defined as follows:

$$(8) \quad l_i(\lambda_\alpha) = \inf\{x : \lambda_\alpha \leq F_i(x)\}.$$

Here $\lambda_\alpha \in \Lambda = [0, 1]$ and $F_i(X)$ is the cumulative distribution function of the beta distribution $\text{Beta}(i, m + 1 - i)$. This family was also considered in Hemerik, Solari and Goeman (2019).

Further examples of candidate critical vector can be found in Blanchard, Neuvial and Roquain (2020), Blanchard, Neuvial and Roquain (2008) and Hemerik, Solari and Goeman (2019), but we did not consider them here. The results obtained with our permutation method will depend on the critical vector $l(\lambda_\alpha)$ and hence on the choice of the family $\mathcal{F} = \{l(\lambda_\alpha) : \lambda_\alpha \in \Lambda\}$. However, one choice of family will essentially never lead to a uniform improvement compared to another family, but only to improved TDP bounds for some sets of hypotheses and worse bounds for other sets of hypotheses. Thus, the most appropriate family will depend on which sets of hypotheses we are most interested in, e.g., on whether we are interested in large or small clusters. Section 6 provides guidelines regarding a good choice of \mathcal{F} for fMRI data.

5. Choice of permutations and t-statistic. The correlation between the sequence of cognitive stimuli and BOLD expresses brain activation. The changing hemodynamic impacts the local intensity of the magnetic resonance signal, i.e., the voxel intensity. Therefore, the intensity of each voxel becomes the unit of interest. The inference is then characterized by high spatial correlation and heteroscedasticity across voxels and also across subjects if the between-subjects analysis is considered, due to different backgrounds, e.g., quality of the recording. The permutation approach is useful in this situation, where parametric tests fail due to violations of assumptions.

In this Section, we review which permutation test is valid and powerful to perform fMRI group analysis consisting of multi-subject studies to explore the differences in BOLD response recorded under two experimental conditions (Holmes et al., 1996; Winkler et al., 2014; Helwig, 2019). Group fMRI data are widely analyzed using a two-stage summary statistics approach within a mixed model. This approach uses ordinary least squares (OLS) methods (Mumford and Nichols, 2009), in particular often one- or two-sample t-tests, using within-subject parameter estimates as observations.

Let the first level within-subject model:

$$\mathbf{Y}_j = X_j \boldsymbol{\beta}_j + \boldsymbol{\epsilon}_j \quad 1 \leq j \leq J$$

where $\mathbf{Y}_j \in \mathbb{R}^n$ is the brain signal of subject j , n is the total number of time points, $X_j \in \mathbb{R}^{n \times p}$ is the design matrix, p is the total number of regressors of interest, and $\boldsymbol{\epsilon}_j \in \mathbb{R}^n$ is the vector of autocorrelated and non-independent error terms. Let $\boldsymbol{\beta}_{1j}$ be the parameter relative to the first experimental condition, while $\boldsymbol{\beta}_{2j}$ to the second experimental condition for the subject j . We make inference on the contrasts of parameter estimates involving brain activation differences, i.e., $\mathbf{D}_j = \hat{\boldsymbol{\beta}}_{1j} - \hat{\boldsymbol{\beta}}_{2j} \in \mathbb{R}^m$, so:

$$\mathbf{D}_j = \boldsymbol{\mu} + \boldsymbol{\epsilon}_j$$

where $\boldsymbol{\mu} \in \mathbb{R}^m$ is the unknown parameter of interest representing the vector of between-subject means, and $\boldsymbol{\epsilon}_j \in \mathbb{R}^m$ is the vector of independent and identically distributed error terms $\sim (0, \Sigma)$. In order to make inference on $\boldsymbol{\mu}$, the one-sample t-test is performed:

$$(9) \quad \mathbf{T} = \frac{\hat{\boldsymbol{\mu}}}{\sqrt{\hat{\sigma}^2/J}}$$

where $\mathbf{T} \in \mathbb{R}^m$, $\hat{\boldsymbol{\mu}}$ equals $\sum_{j=1}^J \mathbf{D}_j / J$ and $\hat{\sigma}$ equals $\sum_{j=1}^J (\mathbf{D}_j - \hat{\boldsymbol{\mu}})^2 / (J - 1)$. So, we have m statistical tests to analyze $H_i : \mu_i = 0$, that create a statistical brain mapping.

Nevertheless, we need valid permutations to have a valid permutation testing procedure. It needs a null-invariant transformation of the data, i.e., the joint distribution of the p-values under H_0 does not change (Hemerik and Goeman, 2018). In this case, $H_i : \mu_i = 0$ implies that $(\boldsymbol{\beta}_{1j}, \boldsymbol{\beta}_{2j}) \stackrel{d}{=} (\boldsymbol{\beta}_{2j}, \boldsymbol{\beta}_{1j})$, that is equivalent to $\mathbf{D}_j \stackrel{d}{=} -\mathbf{D}_j$. The compound symmetry is weaker than normality and also allows for heteroskedasticity. It can be justified by subtraction of two sample means with the same (arbitrary) distribution. Therefore, under H_0 , we can flip the sign at random of each \mathbf{D}_j (Winkler et al., 2014), always taking the identity permutation as the first transformation to have an exact α method (Hemerik and Goeman, 2018; Pesarin and Salmaso, 2010).

The same approach can be used in the case of two-sample t-test. Let $G_j = \{1, 2\}$ expresses the group label for the j -th subject, the null hypothesis is then defined as $H_0 : \mu_{1i} = \mu_{2i}$. The exchangeability assumption implies $(\mathbf{D}_j | G_j = 1) \stackrel{d}{=} (\mathbf{D}_j | G_j = 2)$, we can just shuffle the subject-group labels at random to compute the p-values null distribution. Permutation-based tests can be applied in various hypothesis testing's situations, e.g., tests for linear models even in the presence of nuisance effects (Winkler et al., 2014; Helwig, 2019; Solari, Finos and Goeman, 2014), and tests for generalized linear models (Hemerik, Goeman and Finos, 2020).

6. fMRI data Application. In this Section, permutation-based ARI method is evaluated using fMRI data. Two datasets from <https://openfmri.org/> are analyzed. Both datasets have the same experimental design, i.e., a block design with two stimuli. Pre-processing and first-level data analysis were performed using FSL (Jenkinson et al., 2012). Registration to MNI space was done using FLIRT (Jenkinson and Smith, 2001; Jenkinson et al., 2012), motion correction using MCFLIRT (Jenkinson et al., 2002), and brain-extraction using BET (Smith, 2002). We applied spatial smoothing using a Gaussian Kernel of 6mm FWHM. Finally, we applied a high-pass filter to the time-series data (Gaussian-weighted least-squares straight-line fitting, with $\sigma=64.0s$). The parameter estimates (copes), i.e., D_j , were used as input in the p_{ARI} (Andreella, 2020) package developed in R (R Core Team, 2017).

For all the analyses, the α level is taken as 0.05 for a two-sided alternative hypothesis. We use 1000 permutations: 999 random permutations plus the identity.

We chose δ as 0, 1, 9, and 27, to account for signal spreading out in clusters with size at least equals 0, 1, 9 and 27 voxels. The third powers were considered in order to exploit the three-dimensional structure of the voxels. The results for $\delta = 0$ are used in the primary analyses.

The computation time for each dataset is approximately 220 seconds, more than in Section 3 since we have a larger number of 150,000 hypotheses. Still, computation time is short for a permutation-based method.

6.1. Auditory Data. We analyzed data from 140 subjects passively listening to vocal (i.e., speech), and non-vocal sounds, collected by Pernet et al. (2014), available at <https://openneuro.org/datasets/ds000158/versions/1.0.0>. We estimated the statistics map regarding the contrast that describes the difference of neural activation during vocal and non-vocal stimuli for each participant. These maps, i.e., D_j , were used as input in the permutation-based ARI procedure. The hypothesis testing is then constructed considering $H_0 : \mu_i = 0$ with two-sided alternative, where μ_i is the mean $\sum_{j=1}^J \beta_{\text{vocal } j} - \beta_{\text{no vocal } j} / J$ computed for each voxel $i = 1, \dots, m$, as described in Equation (9).

In concordance with results from earlier studies, we found activation on the Planum Temporale (PT), Superior Temporal Gyrus (STG), Heschl’s Gyrus (HG), Inferior Frontal Gyrus (IFG), Precentral Gyrus (PrG), Paracingulate Gyrus (PG), and Thalamus (T). While our method allows any method for forming clusters, we started from a map computed using Random Field Theory (RFT) with a cluster-forming-threshold equalling $Z > 3.2$. This threshold is quite liberal, and therefore we will make additional inferences inside these clusters with a threshold of $Z > 4$.

Table 1 includes the lower bounds of the proportion of active voxels ($\bar{\pi}(S) = \bar{a}(S)/|S|$), the size of the cluster ($|S|$), the FWER-corrected p-values (p_{FWER}) from classical cluster analysis and the coordinates of the maximum. The FWER p-values based on the Random Field Theory (RTF) are reported only for the first cluster-forming-threshold equals to $Z > 3.2$, since this method does not allow double-dipping. The results are computed using the permutation-based ARI with the Simes and AORC family using $\delta = 0$. We compared these methods with the original parametric ARI calculated using the R package `ARIbrain` (Finos et al., 2018).

As can be seen permutation-based ARI, i.e., columns 10 for the Simes family and 11 for the AORC family in Table 1, has a better performance overall than the parametric approach, i.e., column 12 in Table 1. However, the two families of candidate curves return very similar results; this likely reflects the similar structure of these two families of critical vectors. We also applied the shifted versions with $\delta > 0$ (see Supplementary Material Section for the results), but found that the loss of power in small clusters is not sufficiently offset by a gain

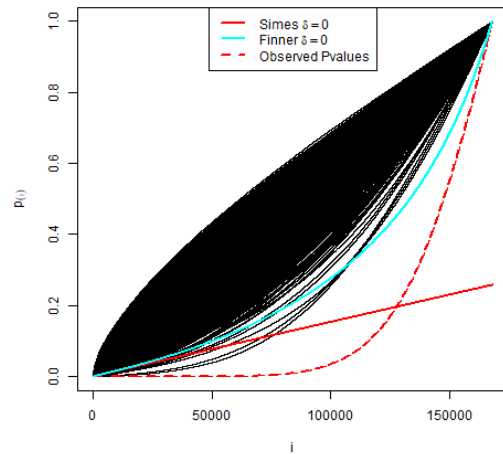


FIG 3. Auditory data: P -values null distribution.

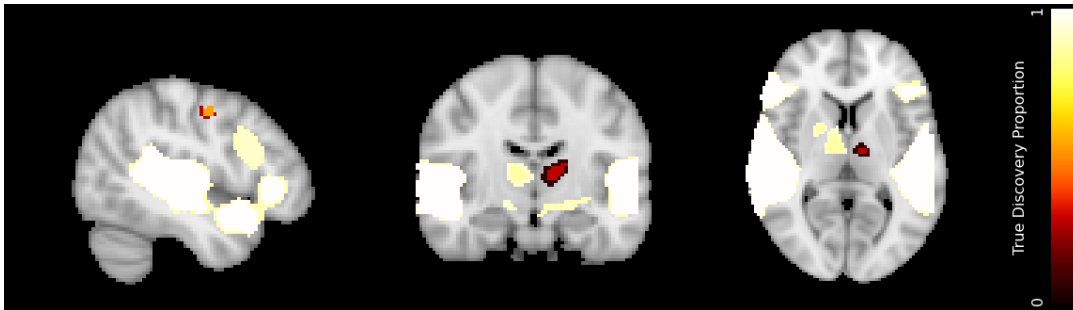


FIG 4. Auditory data: True Discovery Proportion map using the un-shifted Simes family of critical vectors and clusters referred to a threshold equals 3.2 and “drilled” down at 4.

in power in the larger clusters. We believe that this is due to conservativeness of the null p -values as shown in Figure 3. The family of critical vectors based on the Higher Criticism and the Beta quantiles gave very poor results, which we believe is due to mismatch between the design of the curves based on independent p -values that contrasts with a high correlation in the actual data.

Figure 4 shows the TDP bounds as a cluster brain map using the results using the Simes family confidence bound. In these maps the user can directly interpret activation as the proportion of truly active voxels inside a cluster.

6.2. Food Data. Subsequently, we analyzed data from 29 subjects passively looking at food and non-food images, collected by [Smeets et al. \(2013\)](https://openneuro.org/datasets/ds000157/versions/00001) available at <https://openneuro.org/datasets/ds000157/versions/00001>. The analysis follows directly the one performed in Section 6.1, but the difference in neural activation during food and not food stimuli was analyzed.

We found activity in the Amygdala (A), Insular Cortex (IC), Putamen (P), Inferior Frontal Gyrus (IFG), Occipital Pole (OP), Superior Frontal Gyrus (SFG), Frontal Orbital Cortex (FOC), and Postcentral Gyrus (PG). The cluster map is thresholded the same as the previous dataset: using RTF with a threshold of $Z > 3.2$. We then drilled down $\bar{\pi}(S)$ using a threshold of $Z > 4$.

TABLE 1
Auditory data: Clusters identified with threshold $\mathbf{T} > 3.2$ and Active Proportion Percentage, “drill down” clusters at $\mathbf{T} > 4$.

Cluster	Threshold	Size	% active			RFT P-Values p_{FWER}	Voxel Coordinates		
			Perm Simes (10)	Perm AORC (11)	Parametric Simes (12)		x	y	z
S	t	$ S $	$\bar{\pi}(S)$	$\bar{\pi}(S)$	$\bar{\pi}(S)$				
Right STG/PT HG/IFG/T	3.2	11683	92.36%	92.44%	84.98%	< 0.0001	16	59	37
Right STG/PT HG/IFG/T	4	8875	99.54%	99.54%	98.5%	—	16	59	37
Right IFG	4	422	91.47%	91.5%	83.18%	—	20	64	71
Right T	4	292	85.96%	86.3%	64.04%	—	41	59	41
Right T	4	15	13.33%	13.33%	0%	—	39	52	34
Left STG/PT HG/IFG	3.2	7671	88.88%	88.9%	79.96%	< 0.0001	76	58	38
Left STG/PT/HG	4	5448	99.25%	99.27%	97.67%	—	76	58	38
Left IFG	4	515	92.04%	92.23%	79.81%	—	66	71	50
PG	3.2	269	33.09%	33.46%	19.7%	0.0023	44	89	30
PG	4	128	69.53%	70.31%	41.41%	—	44	89	30
Left T	3.2	176	7.96%	8.52%	0.57%	0.0156	53	57	42
Left T	4	49	28.57%	30.61%	2.04%	—	53	57	42
Left T	4	34	50%	50%	29.41%	—	53	51	35
Left PrG	3.2	47	27.66%	27.66%	25.53%	0.387	70	60	61
Left PrG	4	24	54.17%	54.17%	50%	—	70	60	61

Figure 5 shows the null distribution of the p-values from the one-sample t-test (two-sided alternative) for the contrast between food and non-food stimuli. As in Section 6.1, the Table 2 represents the results using the Simes family in column 13, and the AORC family in column 14 with δ equalling 0. As can be seen the power improvement over the parametric method, i.e., column 15 of Table 2, is striking in this data set. For the shifted version of the Simes and AORC family (in the Supplementary materials) we found as in the Auditory data analysis that the δ parameter is not able to capture the active voxels in clusters with a small size, and the non-shifted version is preferred. Once again, the critical vectors based on Higher Criticism and the Beta distribution dos not work well due to the high correlation in the data.

Finally, Figure 6 shows the TDP represented in Table 2 as cluster brain map.

7. Validating Permutation-based ARI. In the fMRI framework, the null data consists of resting-state fMRI data, where the null hypothesis of mean zero activation between-group is true, due to not containing consistent BOLD activity. Eklund, Nichols and Knutsson (2016) found that many software programs, as FSL and SPM (Penny et al., 2011), do not control properly the probability or the average proportion of the false positives in the cluster-wise inference of brain activity, caused by the assumption of spatial autocorrelation having squared exponential shape required for the Gaussian RTF. However, ARI does not make this assumption; for that, we want to analyze the false positive rate of the permutation-based ARI using resting-state fMRI data with no signal from Oulu data provided by the 1000 Functional Connectomes Projects (Biswal et al., 2010).

The Oulu data consists of 103 subjects; however, to estimate the false positive rate, this set of subjects is not sufficient. In addition, Eklund, Nichols and Knutsson (2016) found asymmetric errors in the case of permutation test for the one-sample t-test using the Oulu data; therefore, we validate the permutation-based and parametric ARI, performing the two-sample t-tests. We select two groups of 20 subjects by randomly permuting 1000 times the subject numbers and selecting the first 40 of this permuted data set. Eklund, Nichols and

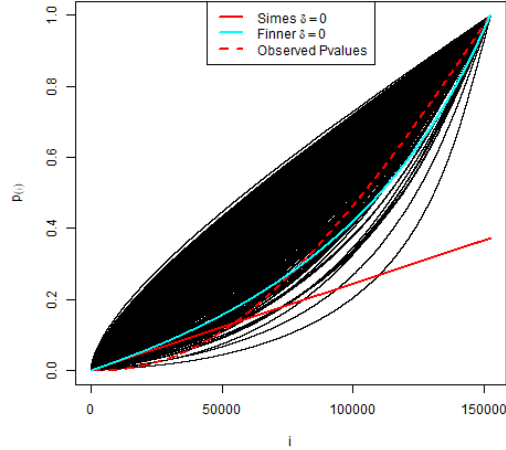


FIG 5. Food data: P-values null distribution.

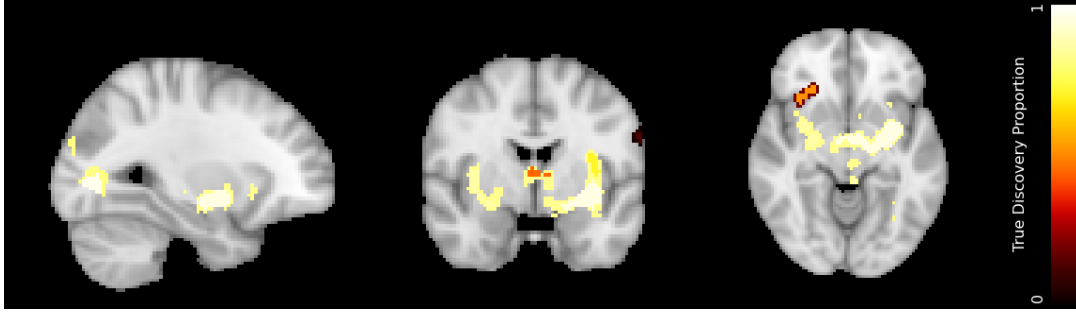


FIG 6. Food data: True Discovery Proportion map using the non-shifted Simes family of critical vectors and clusters referred to a threshold equals 3.2 and “drilled” down at 4.

[Knutsson \(2016\)](#) underlines that the estimate of the false positive rate is unbiased, even if these random datasets aren’t independent. Finally, the set of voxels used as a cluster map is the whole-brain mask.

Using the parametric-based ARI, the false positive rate estimate equals 0, having no dataset with at least one discovery. The permutation-based ARI returns 44 datasets with at least one discovery, i.e., the false-positive rate estimate equals 4.4.%. The mean of $\bar{a}(S_m)/S_m$ over the 1000 simulations equals 0.0063. Therefore, both methods control the FWER as expected.

8. Simulation study. We simulate data considering the simple following model:

$$\mathbf{Y}_i = \boldsymbol{\mu} + \boldsymbol{\epsilon}_i$$

where $\mathbf{Y}_i \in \mathbb{R}^m$, with $i = 1, \dots, n$, n is the number of independent observation and m is the total number of variables. The noise $\boldsymbol{\epsilon}_i \in \mathbb{R}^m$ follows the standard normal distribution with mean 0 and equi-correlation variance structure, i.e., $\boldsymbol{\epsilon}_i \sim \mathcal{N}(0, \Sigma_{\rho^2})$, where ρ is the level of equi-correlation between pairs of variables. The signal $\boldsymbol{\mu}$ is computed considering the difference in means having power of the one-sample t-test equals 0.8. The signal $\boldsymbol{\mu}$ is equal to 0 under the null hypothesis.

First of all, we want to understand how the improvement of the nonparametric TDP lower bound changes concerning ρ and the proportion of null hypotheses ν . Let $n = 50$, $m =$

TABLE 2
Food data: Clusters identified with threshold $\mathbf{T} > 3.2$ and Active Proportion Percentage, “drill downing” clusters at $\mathbf{T} > 4$.

Cluster	Threshold	Size	% active			RFT	Voxel		
			Perm	Perm	Parametric	P-Values	Coordinates		
S	t	$ S $	Simes (13)	AORC (14)	Simes (15)	$PFWER$	x	y	z
Left A/IC/P/IFG and Right A	3.2	3331	83.13%	83.49%	36.84%	< 0.0001	62	65	34
Left IC/P	4	557	95.51%	95.51%	71.1%	—	62	65	34
Left A	4	295	91.53%	91.53%	41.36%	—	57	49	39
Right A	4	187	86.63%	86.63%	50.8%	—	30	65	33
Left IC	4	81	70.37%	71.6%	20.99%	—	63	62	45
Left IC	4	45	44.44%	44.44%	4.44%	—	45	63	41
Left IC	4	16	6.25%	6.25%	0%	—	64	65	50
	4	15	6.67%	6.67%	0%	—	50	69	36
OP	3.2	3023	81.61%	81.97%	55.84%	< 0.0001	54	20	49
Right OP	4	1030	97.57%	97.57%	83.4%	—	35	20	49
Left OP	4	804	96.89%	96.89%	79.35%	—	54	20	49
Left SFG	3.2	223	10.76%	10.76%	0%	0.0031	50	79	65
Left SFG	4	48	50%	50%	0%	—	50	79	65
Right FOC	3.2	134	18.66%	18.66%	0%	0.0287	31	76	33
Right FOC	4	49	51.02%	51.02%	0%	—	31	76	33
Left PG	3.2	41	2.44%	2.44%	0%	0.453	76	63	52
Left PG	4	8	12.5%	12.5%	0%	—	76	63	52

1000, $\rho^2 \in \{0, 0.01, \dots, 0.99, 1\}$ and $\nu \in \{0.6, 0.7, 0.8, 0.9\}$, we simulate data 1000 times and the mean of $\bar{\pi}(S_m)$ over simulation is represented. The Simes family of confidence bound without shift is taken into account to compare with the parametric approach directly. Having no prior knowledge about the structure of the set of hypotheses to analyze, we consider the full set of hypotheses, i.e., S_m . Figure 7 shows the difference of $\bar{\pi}(S_m)$ computed using the permutation and parametric methods over the ρ^2 and ν values. As expected, the permutation approach gets some power respect to the parametric one in the case of correlation between pairs of variables. It can handle any type of dependence structure of the p-values.

Secondly, we want to examine the family of critical curves not applied in Section 6, since the fMRI data are strongly correlated and the p-values distribution results conservative. The Higher Criticism critical vector (7), the Beta critical vector (8) and the Simes critical vector (5) are then used to compute $\bar{a}(S_m)$ using simulated data with $\nu = 0.9$, $m = 1000$ and $n = 50$. As previously, we repeat the simulations 1000 times for each framework, and the mean value of $\bar{a}(S_m)$ is computed. Figure 8 shows the behaviour of these three families of critical vector respect to $\rho^2 \in \{0, 0.01, \dots, 0.99, 1\}$. In Section 4, we said that the Higher Criticism and Beta families could be problematic in the case of a strong correlation between tests. As expected, the Beta critical vector does not work in the case of a strong correlation between variables. Similarly, the Higher Criticism family seems to work, but it loses power with the increase in correlation.

Thirdly, we want to analyze how $\bar{a}(S_m)$, computed using the Simes family of critical curves (5), changes having anti-conservative p-values distribution. We saw that the un-shifted version is preferred in fMRI data, having a conservative distribution of the p-values. Let $n = 50$, $m = 1000$, $\rho = 0$ and $\nu = 0.9$, we compute $\bar{a}(S_m)$ for each 1000 simulations, and once again the mean over simulations is reported. Figure 9 shows $\bar{a}(S_m)$ considering the Simes family using $\delta \in \{0, \dots, 30\}$. We can note that the shifted version works in the case of anti-conservative p-values if the corrected value for the tuning parameter δ is chosen, described by the red dotted line, i.e., $\delta = 8$.

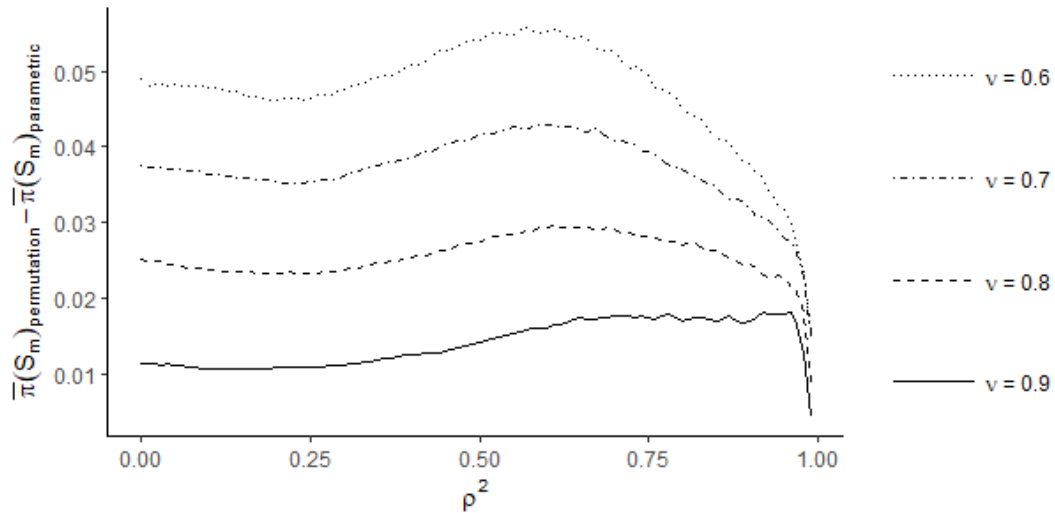


FIG 7. Difference of true discoveries proportion considering the permutation and parametric methods using simulated data and considering the full set of hypotheses S_m over different values of ρ^2 and ν .

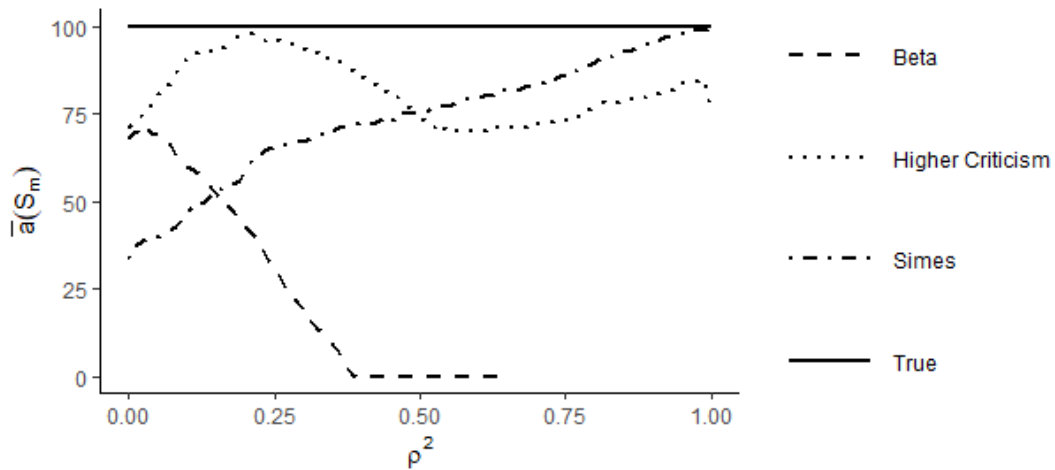


FIG 8. Simulated True Discovery lower bound over S_m and different values of ρ using the Higher Criticism, Beta and Simes critical vectors.

To sum up, we suggest using the Higher Criticism and Beta families if the correlation across the variables is supposed to be low. Besides, we recommend considering the shifted version of the Simes or AORC family if the distribution of the p-value is expected to be anti-conservative, using a reasonable prior value of δ with respect to the data analyzed.

9. Discussion. Our proposed method finds simultaneous lower bounds for the TDP over all possible hypotheses subsets using the permutation theory in a computationally efficient way. As a simultaneous method, it allows the decision of which hypotheses sets to analyze to be entirely flexible and post-hoc, that is, the user can choose it after seeing the data and revise the choice as often as he/she wants. It is particularly useful in the fMRI and MRI multi and

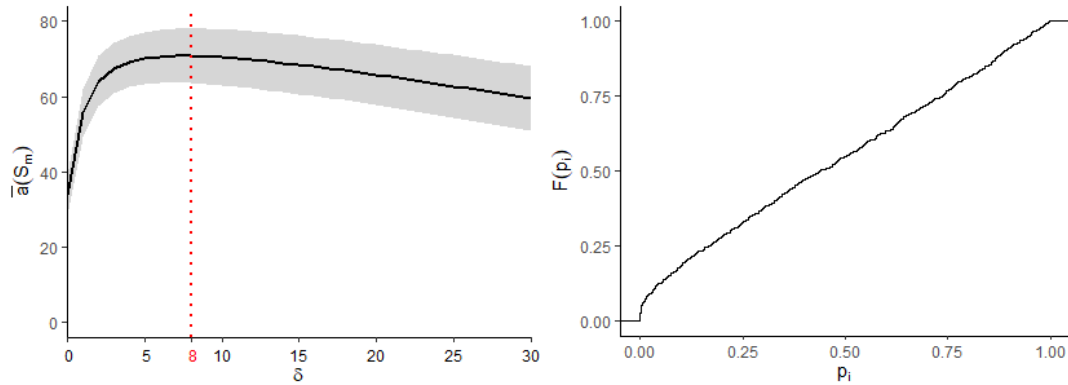


FIG 9. *Left side: True Discovery Lower Bound using simulated data. The full set of hypotheses S_m is considered over different values of δ . Right side: Empirical Cumulative Density Function of observed raw p -values, i.e., $F(p_i)$.*

single subjects analysis to infer inside the clusters, resolving the so-called spatial specificity paradox, without falling into the double-dipping problem.

Permutation-based methods are recommended whenever they can be used, gaining power over the parametric approaches, especially when the p -values are strongly dependent, as for fMRI data. In this work, we used permutation theory to calculate the critical vector needed for ARI. Our method adapts to the correlation structure of the data in an exact way, by means of calibration of the parameter λ_α . In this way, our method remedies existing issues of anti-conservativeness and conservativeness. Indeed, we found that the permutation-based method has more power than the parametric approach both in simulated and real data and confirmed FWER control using resting-state null data.

Permutation methods are not assumption-free but require exchangeability of the test statistics under the null hypothesis. We suggest to use the OLS one-sample t-test for fMRI group analysis, having fast and straightforward computation of the permutation null distribution, randomly flipping the sign of each subject's contrast. The exchangeability assumption needed to perform permutation-based methods is satisfied, i.e., the error terms of the model need to be symmetric around 0. Even if permutations are employed to perform the method proposed, the computation time remains low, e.g., around 200 seconds having 150000 hypotheses and 1000 permutations. The computation time is related to a device with a processor having 1.8 GHz CPU and 16 GB of RAM, finally, the R package `pARI` (Andreella, 2020) based on the C++ language was used.

The proposed method is general, allowing different families of confidence bounds. The choice of the family is critical since it directly influences the bounds for the true discovery proportions, and thus the power properties of the method. We analyzed several such families and found that those based on Simes and AORC are preferred to analyze the group difference between two stimuli in the fMRI framework, imposing a shift parameter δ equal to 0. Shifted versions seemed attractive but lose power in practice, especially for small clusters. In simulated data, we found that the shifted versions gain power if the raw p -values are anti-conservative. Other types of families that we analyzed, based on Higher Criticism (Donoho and Jin, 2004) and Beta quantiles, do not seem to work well in fMRI data analysis due to the strong correlation among the voxels, as also illustrated in the simulation study of Section 8. Generally, we suggest a family of critical vectors more concentrated on small p -values if the number of rejected hypotheses may be low, and a family of critical vectors more diffuse if the number of rejected hypotheses may be high.

The method proposed does not fully generalize upon the method of Hemerik, Solari and Goeman (2019), since we did not implement the iterative approach. There is a potential power gain here, but for fMRI data with sparse signal, the gain is small and comes at a very large computational cost. Our presently used method already provides a substantial power gain with respect to the parametric approach. It provides useful and practical selective inference for fMRI data that exploits the advantages of permutation theory and the closed-testing procedure, resolving the spatial specificity paradox with quite fast computation time.

SUPPLEMENTARY MATERIAL

Supplementary material for “Permutation-based true discovery proportions for fMRI cluster analysis”. In the supplementary material, we provide the proof to Proposition 1. Besides, we provide additional results for permutation-based ARI. In particular, the lower bounds for the TDP are computed in the data examples using the shifted version of the Simes and AORC family, and an additional dataset from Duncan et al. (2009) is analyzed.

REFERENCES

- ANDREELLA, A. (2020). pARI: Permutation-based All-Resolutions Inference. <http://doi.org/10.5281/zenodo.4275924>.
- BENJAMINI, Y. and HOCHBERG, Y. (1995). Controlling the false discovery rate: a practical and powerful approach to multiple testing. *Journal of the Royal statistical society: series B (Methodological)* **57** 289–300.
- BISWAL, B. B., MENNES, M., ZUO, X. N., GOHEL, S., KELLY, C., SMITH, S. M., BECKMANN, C. F., ADLSTEIN, J. S., BUCKNER, R. L., COLCOMBE, S., DOGONOWSKI, A. M., ERNST, M., FAIR, D., HAMPSON, M., HOPTMAN, M. J., HYDE, J. S., KIVINIEMI, V. J., KOTTER, R., LI, S. J., LIN, C. P., LOWE, M. J., MACKAY, C., MADDEN, D. J., MADSEN, K. H., MARGULIES, D. S., MAYBERG, H. S., MCMAHON, K., MONK, C. S., MOSTOFSKY, S. H., NAGEL, B. J., PEKAR, J. J., PELTIER, S. J., PETERSEN, S. E., RIEDL, V., ROMBOUTS, S. A., RYPMA, B., SCHLAGGAR, B. L., SCHMIDT, S., SEIDLER, R. D., SIEGLE, G. J., SORG, C., TENG, G. J., VEIJOLA, J., VILLRINGER, A., WALTER, M., WANG, L., WENG, X. C., WHITFIELD-GABRIELI, S., WILLIAMSON, P., WINDISCHBERGER, C., ZANG, Y. F., ZHANG, H. Y., CASTELLANOS, F. X. and MILHAM, M. P. (2010). Toward discovery science of human brain function. *Proceedings of the National Academy of Sciences* **107** 4734–4739.
- BLANCHARD, G., NEUVIAL, P. and ROQUAIN, E. (2008). Two simple sufficient conditions for FDR control. *Electronic Journal of Statistics* **2** 963–992.
- BLANCHARD, G., NEUVIAL, P. and ROQUAIN, E. (2020). Post hoc false positive control for structured hypotheses. *Scandinavian Journal of Statistics* **47** 1114–1148.
- DONOHO, D. and JIN, J. (2004). Higher criticism for detecting sparse heterogeneous mixtures. *The Annals of Statistics* **32** 962–994.
- DUNCAN, K., PATTAMADILOK, C., KNIERIM, I. and DEVLIN, J. (2009). Word and object processing. *Stanford Digital Repository*. Available at: <http://purl.stanford.edu/nb256hg3654> and <https://openfmri.org/dataset/ds000107/>.
- EKLUND, A., NICHOLS, E. T. and KNUTSSON, H. (2016). Cluster failure: Why fMRI inferences for spatial extent have inflated false-positive rates. *Proceedings of the national academy of sciences* **113** 7900–7905.
- FINNER, H., DICKHAUS, T. and ROTERS, M. (2009). On the false discovery rate and an asymptotically optimal rejection curve. *The Annals of Statistics* **37** 596–618.
- FINOS, L., GOEMAN, J. J., WEEDA, W., ROSENBLATT, J. and SOLARI, A. (2018). ARIBrain: All-Resolutions Inference R package version 0.1.
- GOEMAN, J. J., HEMERIK, J. and SOLARI, A. (2019). Only Closed Testing Procedures are Admissible for Controlling False Discovery Proportions. *arXiv preprint arXiv:1901.04885*.
- GOEMAN, J. J. and SOLARI, A. (2011). Multiple testing for exploratory research. *Statistical Science* **26** 584–597.
- GOEMAN, J. J., MEIJER, R. J., KREBS, T. J. P. and SOLARI, A. (2019). Simultaneous Control of all false discovery proportions in large-Scale multiple hypothesis testing. *Biometrika* **106** 841–856.
- HELWIG, N. E. (2019). Statistical nonparametric mapping: Multivariate permutation tests for location, correlation, and regression problems in neuroimaging. *Wiley Interdisciplinary Reviews: Computational Statistics* **11** e1457.

- HEMERIK, J. and GOEMAN, J. J. (2018). Exact testing with random permutation. *TEST* **27** 811–825.
- HEMERIK, J., GOEMAN, J. J. and FINOS, L. (2020). Robust testing in generalized linear models by sign flipping score contributions. *Journal of the Royal Statistical Society: Series B (Statistical Methodology)* **82** 841–864.
- HEMERIK, J., SOLARI, A. and GOEMAN, J. J. (2019). Permutation-based simultaneous confidence bounds for the false discovery proportion. *Biometrika* **106** 635–649.
- HOLMES, A. P., BLAIR, R. C., WATSON, J. D. G. and FORD, I. (1996). Nonparametric analysis of statistic images from functional mapping experiments. *Journal of Cerebral Blood Flow and Metabolism* **16** 7–22.
- JENKINSON, M. and SMITH, S. M. (2001). A global optimisation method for robust affine registration of brain images. *Medical Image Analysis* **5** 143–156.
- JENKINSON, M., BANNISTER, P., BRADY, M. and SMITH, S. M. (2002). Improved optimisation for the robust and accurate linear registration and motion correction of brain images. *NeuroImage* **17** 825–841.
- JENKINSON, M., BECKMANN, C. F., BEHRENS, T. E. J., WOOLRICH, M. W. and SMITH, S. M. (2012). FSL. *NeuroImage* **62** 782–790.
- KRIEGESKORTE, N., SIMMONS, W. K., BELLGOWAN, P. S. and BAKER, C. I. (2009). Circular analysis in systems neuroscience – the dangers of double dipping. *Nature Neuroscience* **12** 535–540.
- MARCUS, R., PERITZ, E. and GABRIEL, K. R. (1976). On closed testing procedures with special reference to ordered analysis of variance. *Biometrika* **63** 655–660.
- MEIJER, R. J., THIJMEN, J. P., KREBS, T. J. P. and GOEMAN, J. J. (2019). Hommel’s procedure in linear time. *Biometrical Journal* **61** 73–78.
- MUMFORD, J. A. and NICHOLS, T. (2009). Simple group fMRI modeling and inference. *NeuroImage* **47** 1469–1475.
- NICHOLS, T. and HAYASAKA, S. (2003). Controlling the familywise error rate in functional neuroimaging: a comparative review. *Statistical Methods in Medical Research* **12** 419–446.
- PENNY, W. D., FRISTON, K. J., ASHBURNER, J. T., KIEBEL, S. J. and NICHOLS, T. E. (2011). *Statistical Parametric Mapping: The Analysis of Functional Brain Images*. Elsevier.
- PERNET, C. R., MCALEER, P., LATINUS, M., GORGOLEWSKI, K. J., CHAREST, I., BESTELMEYER, P. E., WATSON, R. H., FLEMING, D., CRABBE, F., VALDES-SOSA, M. and BELIN, P. (2014). The human voice areas: Spatial organization and inter-individual variability in temporal and extra-temporal cortices. *NeuroImage* **119** 164–174.
- PESARIN, F. and SALMASO, L. (2010). *Permutation Tests for Complex Data: Theory, Applications and Software*. John Wiley and Sons.
- ROSENBLATT, J. D., FINOS, L., WOUTER, D. W., SOLARI, A. and GOEMAN, J. J. (2018). All-Resolutions Inference for brain imaging. *NeuroImage* **181** 786–796.
- SARKAR, S. K. (2008). On the Simes inequality and its generalization. *Beyond parametrics in interdisciplinary research: Festschrift in honor of Professor Pranab K. Sen* **1** 231–242.
- SIMES, R. J. (1986). An improved Bonferroni procedure for multiple tests of significance. *Biometrika* **73** 751–754.
- SMEETS, P. A. M., M. KROESE, F. M., EVERS, C. and DE RIDDER, D. T. D. (2013). Allured or alarmed: Counteractive control responses to food temptations in the brain. *Behavioural Brain Research* **248** 41–45.
- SMITH, S. M. (2002). Fast robust automated brain extraction. *Human Brain Mapping* **17** 143–155.
- SOLARI, A., FINOS, L. and GOEMAN, J. J. (2014). Rotation-based multiple testing in the multivariate linear model. *Biometrics* **70** 954–961.
- R CORE TEAM (2017). R: A Language and Environment for Statistical Computing R Foundation for Statistical Computing, Vienna, Austria.
- WINKLER, A. M., RIDGWAY, G. R., WEBSTER, M. A., SMITH, S. M. and NICHOLS, T. E. (2014). Permutation inference for the general linear model. *NeuroImage* **92** 381–397.
- WINKLER, A. M., RIDGWAY, G. R., DOUAUD, G., NICHOLS, T. E. and SMITH, S. M. (2016a). Faster permutation inference in brain imaging. *NeuroImage* **141** 502–516.
- WINKLER, A. M., WEBSTER, M. A., BROOKS, J. C., TRACEY, I., SMITH, S. M. and NICHOLS, T. E. (2016b). Non-parametric combination and related permutation tests for neuroimaging. *Human Brain Mapping* **37** 1486–1511.
- WOO, C. W., KRISHNAN, A. and WAGER, T. D. (2014). Cluster-extent based thresholding in fMRI analyses: pitfalls and recommendations. *NeuroImage* **91** 412–419.